TECHNISCHE UNIVERSITÄT MÜNCHEN

WALTHER-MEISSNER-INSTITUT FÜR TIEF-TEMPERATURFORSCHUNG

BAYERISCHE AKADEMIE DER WISSENSCHAFTEN

Circuit quantum electrodynamics with a transmon qubit in a 3D cavity

Master's Thesis

Gustav Andersson

Supervisor: Prof. Dr. Rudolf Gross

Munich, March 2015

Contents

List of Figures

Chapter 1

Introduction

Quantum information processing is a rapidly advancing field of physics showing great potential for future applications in the computing industry. The fundamental component of quantum information systems is the quantum bit (qubit), a quantum two-level system whose state can be read and manipulated in a controlled manner. Using arrays of such qubits coupled together, quantum superposition and entanglement of states could enable the implementation of certain algorithms providing an immense increase in efficiency as compared to classical computing. The perhaps most famous example is Shor's algorithm for factorizing integers, with potentially great implications for modern cryptography. On an ideal quantum computer, this algorithm finds the prime factors of any integer in polynomial time [1].

Among the most promising candidates for realizing quantum computing are superconducting qubits. These are electric circuits based on the special physical properties of the Josephson junction, a circuit element with a nonlinear inductance [2]. Named after British physicist Brian Josephson, the Josephson junction consists of two superconducting metal electrodes separated by a thin insulating layer, typically a few nanometres thick. The integration of Josephson junctions into electric circuits has given rise to the field circuit quantum electrodynamics (QED). In this field, circuits play the roles of natural atoms and optical cavities in quantum-optical cavity QED. Thanks to the macroscopic nature of quantum phenomena in superconductivity, qubit properties can to a large extent be engineered to meet desired specifications, rather than just relying on the natural properties of atoms or molecules. Using well developed microwave engineering principles, circuit QED enables study of light-matter interaction by coupling qubits to resonant structures, such as coplanar waveguide resonators.

Due to their size, superconducting qubits are difficult to isolate from their environment. The quantum states necessary for quantum computing or other experimental schemes are sensitive to stray fields and thermal noise. The preservation of the quantum properties of the system, coherence, is therefore an important aspect of qubit design. The transmon qubit [3], conceived in 2007, is designed to mitigate this problem by reducing sensitivity to fluctuations in local electric charge density in the sample. This has helped maintain the strong trend in increasing coherence times for superconducting qubit designs.

In recent developments, the planar circuits where the qubit is embedded have been replaced by three-dimensional cavity resonators. Such configurations offer several advantages, in particular towards coherence. As qubits decay from excited states by emitting a photon, the mode volume of the final photon state may significantly affect this process. These so-called 3D transmons therefore combine the high coupling strength of typical superconducting qubits with long coherence times. This is typically challenging to achieve as strong coupling to the cavity fields usually implies strong coupling also to the environment, inducing loss of coherence. Times for excited state qubit decay, commonly denoted T_1, close to $100\,\mu s$ have been recorded [4].

In this thesis, we characterize superconducting cavities for use with transmon qubits. We employ microwave measurement techniques and cryogenics to determine the cavity transmission properties. We proceed to investigate a system with a transmon coupled to a cavity resonator in 3D circuit QED experiments. Using microwave spectroscopy in a dilution refrigerator setup, the qubit parameters and the properties of the combined system are investigated experimentally.

A long-term goal of this project is to extend the qubit-cavity system to a network of two or more resonators, with qubit-mediated interaction. Such a system may allow experimental studies of entangled photon states, where a single photon may be present in different cavities simultaneously. It also shows promise for quantum information processing applications, due to the increased coherence times accessible in cavity resonators. This thesis therefore includes preliminary analysis towards such implementations, mainly from a microwave engineering analysis point of view.

We begin in Ch. 2 by introducing fundamental theoretical concepts regarding superconducting circuits, cavity resonators and light-matter interaction. Having laid the foundation to the investigations carried out in this work, we proceed in Ch. 3 to describe the particulars of the experimental design and setup involved. This section also contains the numerical methods used and the simulation results. The main results obtained are presented in Ch. 4, starting with cavity characterization data. We then outline the results obtained from qubit spectroscopy in single as well as two-tone measurements. Finally, Ch. 5 states our conclusions and provides an outlook.

Chapter 2

Theory

In this section, we introduce the theoretical aspects underlying the experiments carried out and the results presented in this work. The fundamentals of Josephson junctions are discussed, and the relevant energy scales for applications in superconducting circuits are introduced. We outline the principles of superconducting charge qubit circuits and their operation. In particular, the properties and ideas behind the transmon qubit are described.

We also introduce the classical theory of three-dimensional electromagnetic resonators necessary for the investigated implementations. The qubit and resonator theory are then combined to discuss the fundamentals of light-matter interaction in a quantum mechanical picture. These principles are then applied to the parameter range relevant to our experimental configurations.

2.1 Josephson Junctions

A fundamental element in any superconducting qubit design is the Josephson junction, consisting of two superconducting electrodes separated by a thin insulating barrier. In the macroscopic quantum model of superconductivity [5], the density of the superconducting charge carrier component is related to a macroscopic wavefunction of definite magnitude and phase

$$\Psi(\mathbf{r},t) = |\Psi(\mathbf{r},t)| \cdot e^{i\theta(\mathbf{r},t)} = \sqrt{n(\mathbf{r},t)}e^{i\theta(\mathbf{r},t)}. \tag{2.1}$$

The squared magnitude of this wavefunction gives the density $n = n(\mathbf{r},t)$ of the superconducting charge carriers. The presence of a phase θ gives rise to macroscopic quantization and interference phenomena. The origin of this macroscopic state in the formation of electron pairs, called Cooper pairs, of charge $2e$ and spin zero, is explained by the theory of Bardeen, Cooper and Schrieffer (BCS theory) [6].

In a Josephson junction, the separation between two superconducting electrodes is sufficiently small to create a weak coupling between them. The macroscopic superconducting wavefunctions of the electrodes overlap, leading to the tunnelling of Cooper pairs across the barrier. The Josephson junction is so named because of Brian Josephson's prediction of the Josephson relations for this system, in 1962 [7]. The first Josephson equations reads

$$I_s = I_c \sin(\phi)\,. \tag{2.2}$$

This equation, the current-phase relation, describes the supercurrent flow between the electrodes. The relative phase between the superconductors is given by $\phi = \theta_2 - \theta_1$ and I_c is the critical current, the maximum supercurrent the Josephson current can sustain in a zero voltage state. The second Josephson relation concerns the time evolution of the phase difference when a voltage is applied across the junction,

$$\frac{d\phi}{dt} = \frac{2\pi}{\Phi_0} V. \tag{2.3}$$

This equation is known as the voltage-phase relation. The factor Φ_0 entering on the right-hand side is the magnetic flux quantum, and is equal to $h/2e$. The way both current and voltage are related to the phase causes the Josephson junction to act as a non-linear inductance. In electric circuits, inductances are associated with stored magnetic field energy. The Josephson junction likewise accumulates potential energy, but rather than in a magnetic field it is stored in the kinetic energy of the moving electrons [8]. This *Josephson coupling energy* is given by

$$U = \frac{\Phi_0 I_c}{2\pi}\left(1 - \cos\phi\right). \tag{2.4}$$

This energy, whose scale is set by $E_J = \Phi_0 I_c / 2\pi$, will turn out to be important to Josephson junction based qubit schemes. Due to the parallel geometry of the superconducting electrode faces, the Josephson junction also has a capacitance. This gives rise to a capacitive charging energy whenever there is a potential difference across the junction. The relevant scale for this energy is set by $E_C = e^2/2C$, where C is the junction capacitance.

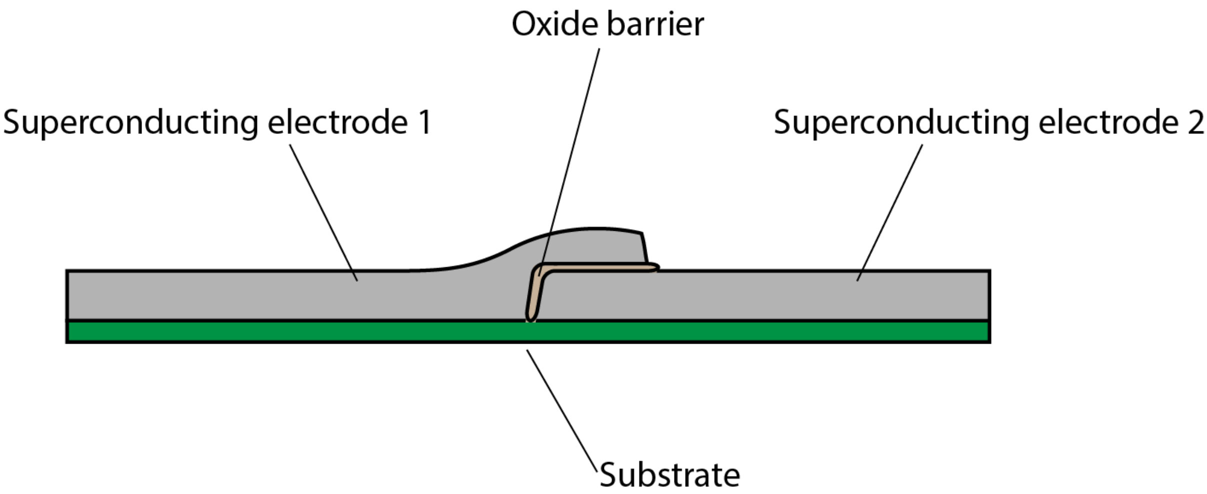

Figure 2.1: Schematic drawing of an SIS Josephson junction. An insulating oxide barrier separates the two superconducting electrodes.

Figure 2.1 shows a schematic drawing of a Josephson junction with a thin oxide tunnel barrier. It is worth noting that although Brian Josephson's original theoretical predictions were made considering a system as described above with a superconductor-insulator-superconductor (SIS) structure, the Josephson relations also hold for other types of weak links between superconductors. Examples include a barrier of normal state, non superconducting metal as well as a constriction in the form of a bottleneck-like narrow section of the superconductor [9].

2.2 Superconducting qubits

When cooled down to sufficiently low temperatures, where $k_B T \ll E_J, E_C$, Josephson junction circuits exhibit quantum properties. The junction charge and phase variables Q and ϕ then have to be replaced by operators, which crucially obey a quantum commutation relation

$$\left[\hat{\phi},\hat{Q}\right] = 2ie. \tag{2.5}$$

The charge operator $\hat{Q}$ is thus canonically conjugate to the phase, similarly to the position and momentum operators, meaning that they are subject to Heisenberg's uncertainty principle. This implies that if ϕ is well defined, Q fluctuates strongly and vice versa. This quantum behaviour is the basis for turning superconducting circuits into qubits.

Any quantum two-level system is analogous to a spin 1/2 system, elegantly described by the Pauli matrices [10]. In this picture, the qubit excited and ground states $|1\rangle$ and $|0\rangle$ are the eigenstates of σ_z. General qubit states in this basis are represented using the Bloch sphere, a unit sphere centered at the origin of a cartesian coordinate system. A point within the enclosed volume corresponds to an expectation value $\mathbf{R} = \langle\vec{\sigma}\rangle$. Qubit operation

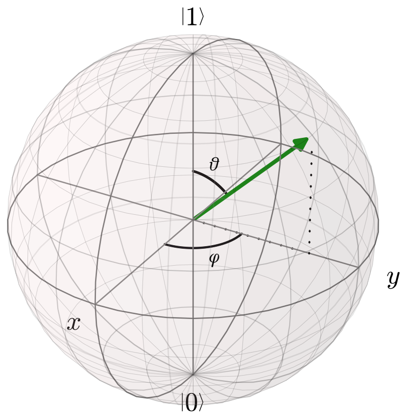

Figure 2.2: Bloch sphere schematic. Pure qubit states $|\psi\rangle$ are often represented in spherical coordinates. In this basis we have $|\psi\rangle = e^{i\varphi} \sin\left(\frac{\vartheta}{2}\right)|0\rangle + \cos\left(\frac{\vartheta}{2}\right)|1\rangle$. The polar coordinates are not to be confused with the superconducting phase variables.

implies manipulation and control of this Bloch vector $\mathbf{R}$. The norm of the Bloch vector is preserved under unitary time evolution and states on the surface of the Bloch sphere ($|\mathbf{R}| = 1$) are possible observable eigenstates. Such a ”pure” state is illustrated in Fig. 2.2. States in the interior $|\mathbf{R}| < 1$ correspond to a statistical mixture, representing a lack of precise knowledge of the quantum state. Such states are probabilistic in a classical sense, not related to quantum uncertainty, and the irreversible time evolution that increases this mixing is one of the major obstacles to successful qubit operation.

The cause of this loss of certainty and the reason we consider it irreversible is that it arises from interaction with the environment, due to the naturally imperfect isolation of the qubit system. Two characteristic timescales are relevant to describe this process. The decay time, $T_1 = 1/\pi\Gamma_1$, is the inverse rate of depopulation of the excited qubit state. The loss of quantum coherence, corresponding to a projection of the Bloch vector onto the $z-$axis, occurs in the characteristic time $T_2 = 1/\pi\Gamma_2$. As states outside the Bloch sphere are unphysical, depopulation must be accompanied by a certain decoherence, leading to the limit $\Gamma_2 \geq \Gamma_1/2$.

2.2.1 The Cooper pair box

The single Cooper pair box (CPB) couples a small superconducting island via a Josephson junction to a gate electrode. Figure 2.3 shows an equivalent circuit diagram. Two characteristic energies are of interest for this system. The capacitive coupling of the island to the environment produces a charging energy when a gate voltage is applied or the island carries excess charge. This island is sufficiently small to make a single Cooper pair the relevant charge scale (hence its name), leading us to introduce the dimensionless charge variable $n = Q/2e$ and modify the charging energy scale $E_C = e^2/2C_\Sigma$ to account

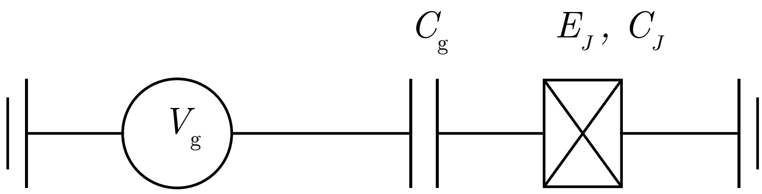

Figure 2.3: Circuit diagram of the Cooper pair box. Charges tunnel onto the island through the Josephson junction, represented by the crossed square.

for the additional capacitance. The total capacitance $C_\Sigma = C_g + C_J$ is the sum of the gate and Josephson junction capacitances. Together with the Josephson energy of Eq. (2.4), we obtain a circuit Hamiltonian

$$\hat{H} = 4E_C\left(\hat{n} - n_g\right)^2 - E_J \cos\hat{\phi}. \tag{2.6}$$

The effective offset charge introduced by the gate bias V_g is $n_g = C_\Sigma V_g/2e$. Using the quantum commutation relation $\left[\hat{n},\hat{\phi}\right] = i$, it is possible to express this Hamiltonian in the charge basis as [11]

$$\hat{H} = 4E_C\left(\hat{n} - n_g\right)^2 - \frac{E_J}{2}\sum_n \left|n+1\right\rangle\left\langle n\right| + \left|n+1\right\rangle\left\langle n\right| \tag{2.7}$$

For qubit operations, the CPB is typically biased at the "sweet spot" $n_g = 1/2$, where the charging energy degeneracy of the $n = 0$ and $n = 1$ states is only broken by the Josephson energy. There are two distinct advantages with this regime. As the charging energy is typically dominant, $E_C \gg E_J$, the higher charge energy levels will be far away, so that a two-level approximation will be valid for the system in this case. In addition, this bias point provides reduced sensitivity to charge noise fluctuations, an important cause of decoherence.

2.2.2 The transmon qubit

The transmon is a qubit design similar to the Cooper pair box. It differs in that a shunt capacitance is added between the gate and the island (cf. Fig. 2.4). By increasing the capacitance of the island, this lowers the charging energy $E_C = e^2/2C$, leading to an increased E_J/E_C ratio. A higher E_J/E_C leads to a more harmonic energy spectrum, and also flattens the charge dispersion. By charge dispersion we mean the relationship between the qubit eigenenergies and offset charge n_g. A steep charge dispersion implies the energies change rapidly with n_g, and vice versa. While a certain anharmonicity is required for the two-level approximation of the qubit to remain valid, a flattened charge dispersion can significantly mitigate the problem of charge noise dephasing. A cricital property to the operation of the transmon is the fact that as E_J/E_C is increased, the charge dispersion is exponentially suppressed, the anharmonicity only reduces by a power law. The result is

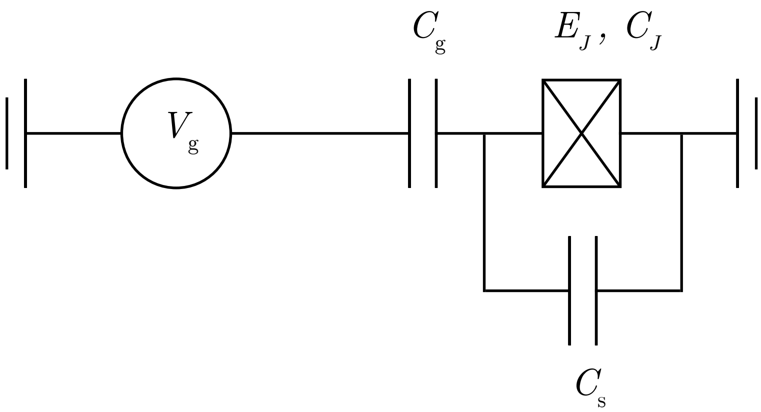

Figure 2.4: The transmon qubit equivalent circuit. Compared to the Cooper pair box, an extra capacitance has been added between the island and ground.

that the n_g-dependence of the energy levels may be practically eliminated, while retaining sufficient anharmonicity for qubit operation. The eigenenergies of the four lowest qubit levels are plotted for different values of E_J/E_C in Fig. 2.5. The energy eigenvalues were obtained using the QuTiP library [12].

Applying second order perturbation theory to find the transmon energies gives for the first two transitions gives [3]

$$E_{01} = \sqrt{8E_C E_J} - E_C \tag{2.8}$$

$$E_{12} = \sqrt{8E_C E_J} - 2E_C \tag{2.9}$$

where E_{01} and E_{12} are the energies of the first and second transitions, respectively. They are related to the corresponding transition frequencies f_{ij} by Planck's constant, $E_{ij} = hf_{ij}$. Transmon qubits are typically designed to operate in the $E_J/E_C \sim 50$ regime. We then get an approximate relative anharmonicity

$$A_{rel} \equiv \frac{E_{01} - E_{12}}{E_{01}} = \sqrt{\frac{E_C}{8E_J}}. \tag{2.10}$$

Though commonly referred to as charge qubits, this term is not entirely consistent with the fact that the Josephson energy dominates over the charging energy in most applications. The flattened charge dispersion of the transmon has an important implication for qubit experiments besides the improved coherence lifetime. Since n_g is not a relevant tuning parameter any more, no bias circuitry is necessary to ensure functional operation. This makes the transmon suitable for applications where control circuits may be impractical to implement. Relevant for this thesis is the three-dimensional configuration enclosing the transmon in a superconducting cavity. Here, we let the shunt capacitance serve also as the antennas necessary for the interaction with the electric field. As seen in the schematic

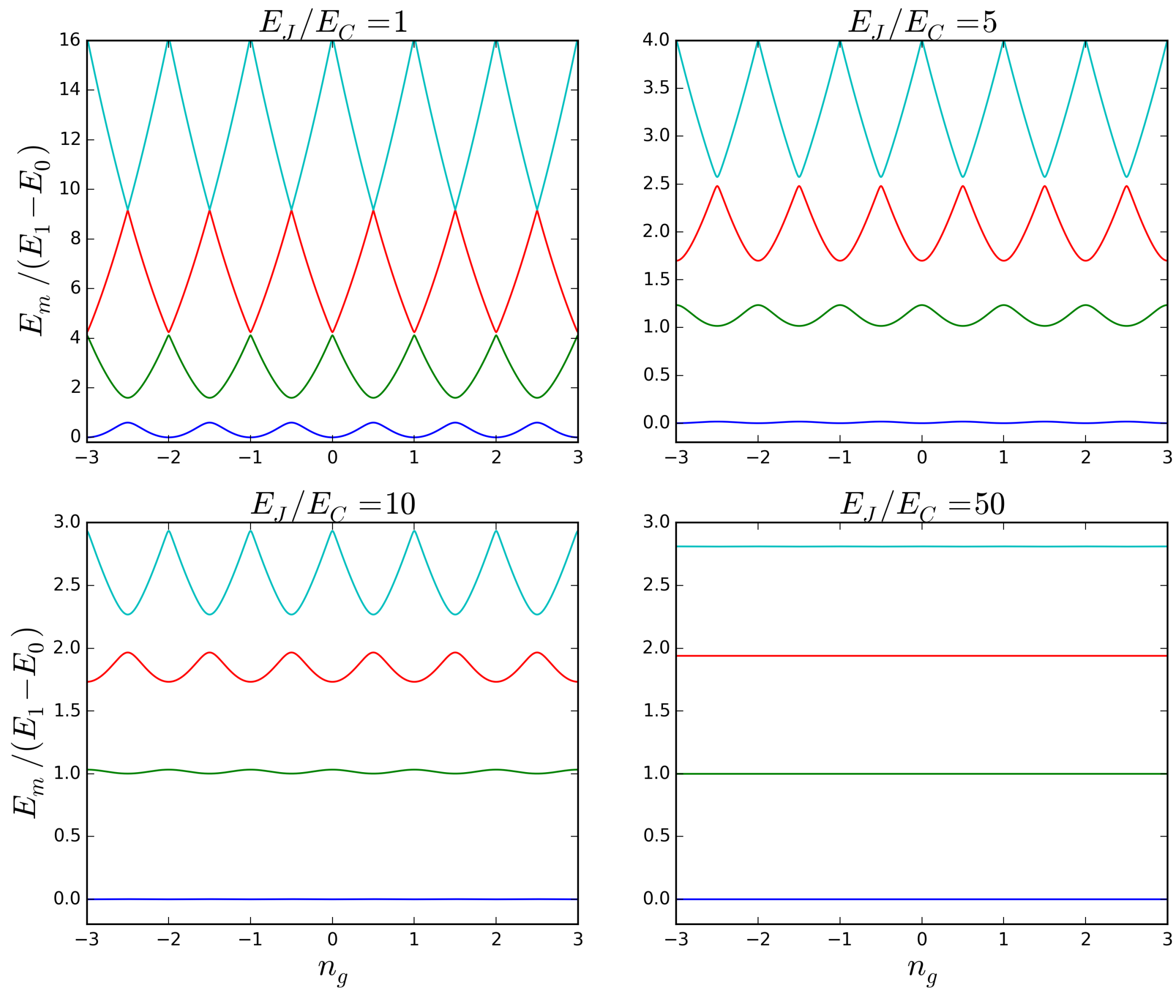

Figure 2.5: The first four energy levels of the charge qubit as a function of n_g, plotted for different values of E_J/E_C. The levels are eigenenergies of the Hamiltonian of Eq. (2.7).

presented in Fig. 2.6, this leads to a design less complex than the equivalent circuit diagram may suggest.

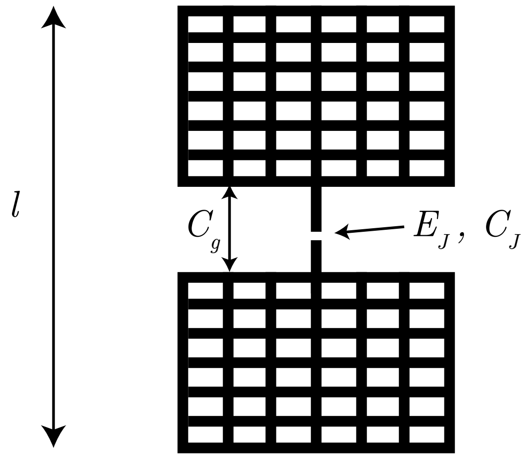

Figure 2.6: Schematic illustration of the 3D transmon design. The pad structures provide the shunt capacitance as well as the resonator coupling. The Josephson junction is marked with the junction energy E_J and junction capacitance E_J. The length of the qubit structure l influences the dipole moment of the structure, which is critical to the electric field coupling.

While the low charging energy of the transmon removes the relevance of a gate bias voltage, a modification enabling tuning of the Josephson energy may substantially expand the scope of possible experiments [13]. This is done by splitting the junction into two symmetric branches, effectively turning it into a loop with two Josephson junctions, commonly known as a superconducting quantum interference device (SQUID) [8]. Flux quantization requires the total flux penetrating the loop be an integer multiple of Φ_0 [8]. An important consequence is an effective change in E_J when an external flux is applied, as screening currents in the loop arise to compensate the bias flux and maintain flux quantization.

The circuit diagram of a tunable transmon is displayed in Fig. 2.7. The split junction has an effective combined capacitance and flux tunable Josephson energy.

2.3 Cavity resonators

A 3D cavity resonator is a vacuum volume enclosed in metal. The eigenmodes of the electromagnetic field in such structures have a dilute field strength and large vacuum participation with a minimum of lossy components inside the mode volume. As a result it is relatively easy to operate such cavities at a low photon loss rate. The damping of the resonator is described by the dimensionless quality factor, or Q-factor, defined as ratio of energy stored in the electromagnetic field to the loss per period of oscillation T, multiplied by a factor of 2π

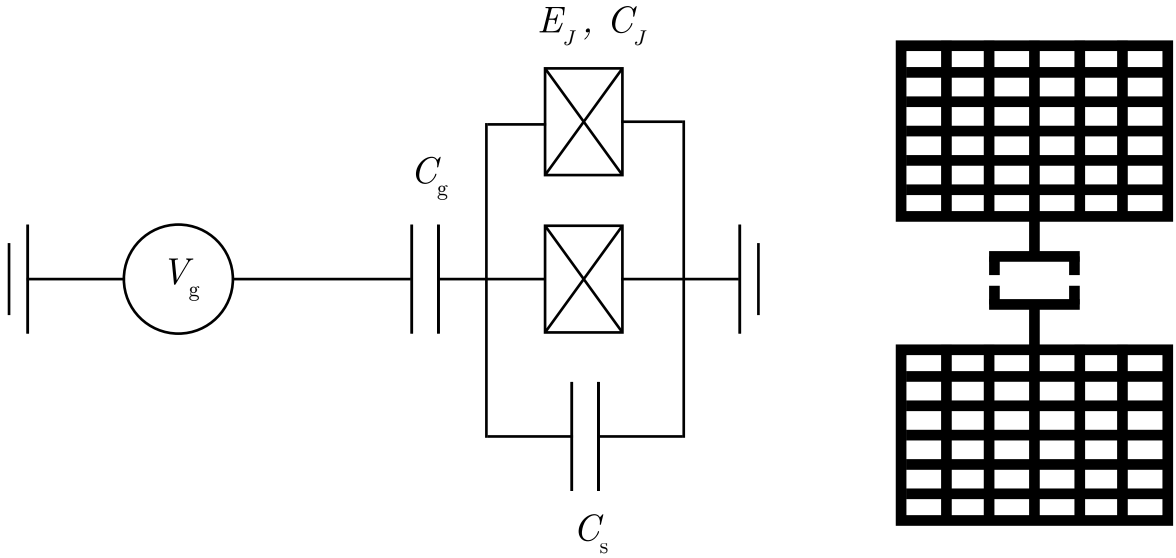

Figure 2.7: Equivalent circuit diagram and 3D schematic design of a tunable transmon. The effective Josephson energy is altered by coupling an external magnetic flux into the split junction loop.

$$Q = \frac{2\pi}{T}\frac{U}{P_d} = \frac{\omega U}{P_d}. \tag{2.11}$$

The stored energy is given by U. The power dissipation due to resonator losses is described by P_d and ω is the angular frequency of the oscillations. In the limit where $Q \gg 1$, the cavity transmission has a Lorentzian lineshape centered at the resonance frequency, with a linewidth determined by the loss rate κ. The Q-factor may then be expressed as

$$Q = \frac{\omega_r}{\kappa} = \frac{\omega_r}{\Delta\omega_r}. \tag{2.12}$$

The resonant bandwidth $\Delta\omega_r = \kappa$ is given by the full width at half maximum (FWHM) of the Lorentzian. This is illustrated in Fig. 2.8. The quality factor may be decomposed into the internal and external quality factors. The internal Q-factor Q_{int} describes internal losses in the metal surface or absorption from two-level systems inside the resonant volume. The external Q-factor Q_{ext} accounts for photons exiting the cavity through the input or output lines that couple the cavity to the environment, in this case the setup electronics. Equation (2.12) gives the total, or loaded quality factor. As the loss rates through different channels add up, and the Q-factor is reciprocal to loss, the total quality may be calculated as

$$\frac{1}{Q} = \frac{1}{Q_{\text{ext}}} + \frac{1}{Q_{\text{int}}}. \tag{2.13}$$

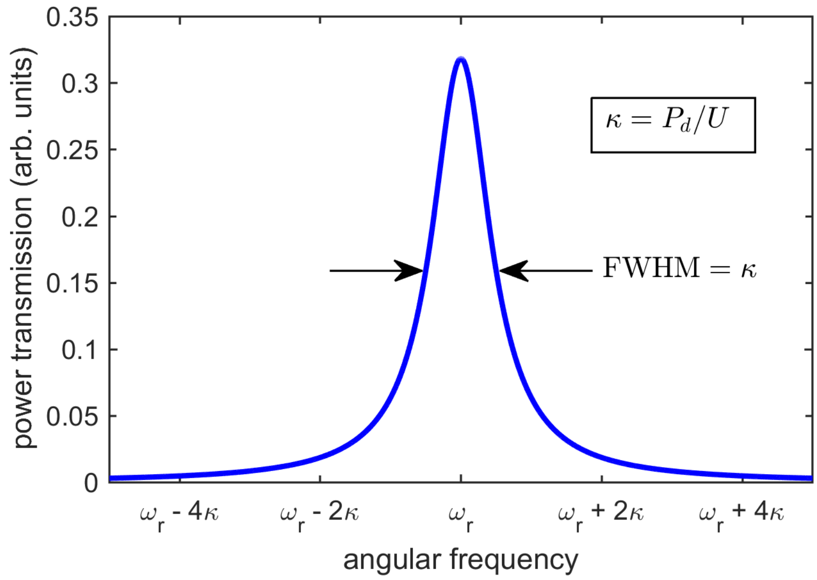

Figure 2.8: The resonator transmission lineshape is a Lorentzian. The bandwidth of the transmission is determined by the loss rate.

Internal loss

The cavity losses that yield the internal quality factor occur mainly in the conducting metal walls, and so depend on the surface resistivity of the material. The power dissipation in the walls is given by [14]

$$P_{\text{walls}} = \frac{R_{\text{s}}}{2} \int_{\text{walls}} |H_{\text{t}}|^2 \, ds. \tag{2.14}$$

The surface resistivity is denoted by R_{s} and H_{t} is the magnetic field tangential to the cavity surface. A common approach to achieve high Q-factors is the use of superconducting cavities, which have minimal surface resistivity. Much of the development towards low-loss resonators and other superconducting radio frequency applications has been done within accelerator physics, aiming at methods to efficiently accelerate charged particles. An expression for the surface resistivity can be formulated using BCS theory [15]

$$R_{\text{s}} = R_{\text{BCS}} + R_{\text{res}} \tag{2.15}$$

where R_{BCS} is the BCS surface resistivity, up to a prefactor given by

$$R_{\text{BCS}} \propto \frac{\omega^2}{T} e^{-1.76 T_c/T}. \tag{2.16}$$

Dissipation occurs due to oscillations in normal-component electrons induced by the penetration of the magnetic field into the metal. The density of electrons not bound in

Cooper pairs decreases exponentially with T_c/T, where T_c is the superconducting critical temperature. The other term in the total surface resistivity is the residual resistivity R_{res}. It is associated with surface imperfections, such as lattice distortions and defects, as well as trapped magnetic flux. The surface resistivity is independent of temperature, but surface treatment approaches such as electropolishing have been shown to reduce this component [16]. Apart from losses to the cavity walls, internal losses may arise from absorption due to two-level systems in dielectrics present within the mode volume, such as the qubit chip substrate.

Cavity modes

We seek to fit a transmon qubit inside an approximately rectangular cavity. The lowest electromagnetic field modes of such a cavity and the ones relevant for our qubit experiments are the TE_{10l} modes, l = 1,2. In this context, TE stands for transverse electric, meaning the electric field is everywhere perpendicular to the direction of propagation. Letting the polarization define the y-axis gives $\mathbf{E} = E_y\mathbf{e}_y$. In a rectangular cavity resonator, the electric field of the TE_{10l} modes is then given by [14]

$$E_y = E_0 \sin\left(\frac{\pi x}{a}\right)\sin\left(\frac{l\pi z}{d}\right). \tag{2.17}$$

The first two modes are visualized in Fig. 2.9. The fundamental mode has an electric field anti-node in the cavity center and the length of the cavity corresponds to $\lambda/2$, meaning there is one standing wave antinode in the propagation direction. The second cavity mode has two standing wave antinodes along the length of the cavity d, does however not correspond to twice the frequency of the first mode.

Scattering parameters

The transmission and reflection amplitudes of signals coupled into the cavity are often described using scattering parameters, or S-parameters. Generally, S-parameters describe the propagation of electrical signals between ports in a network and are represented as a matrix [14]:

$$\begin{bmatrix} V_1^- \\ V_2^- \\ \vdots \\ V_n^- \end{bmatrix} = \begin{bmatrix} S_{11} & S_{12} & \cdots & S_{1n} \\ S_{21} & S_{22} & \cdots & S_{2n} \\ \vdots & \vdots & \ddots & \vdots \\ S_{N1} & S_{N2} & \cdots & S_{NN} \end{bmatrix} \begin{bmatrix} V_1^+ \\ V_2^+ \\ \vdots \\ V_n^+ \end{bmatrix} \tag{2.18}$$

The incident voltage signal at port i is given by V_i^+ and V_i^- represents the outgoing amplitude at the same port. The individual matrix elements S_{ij} may be determined by exciting port j while terminating all others except port i with no impedance mismatch.

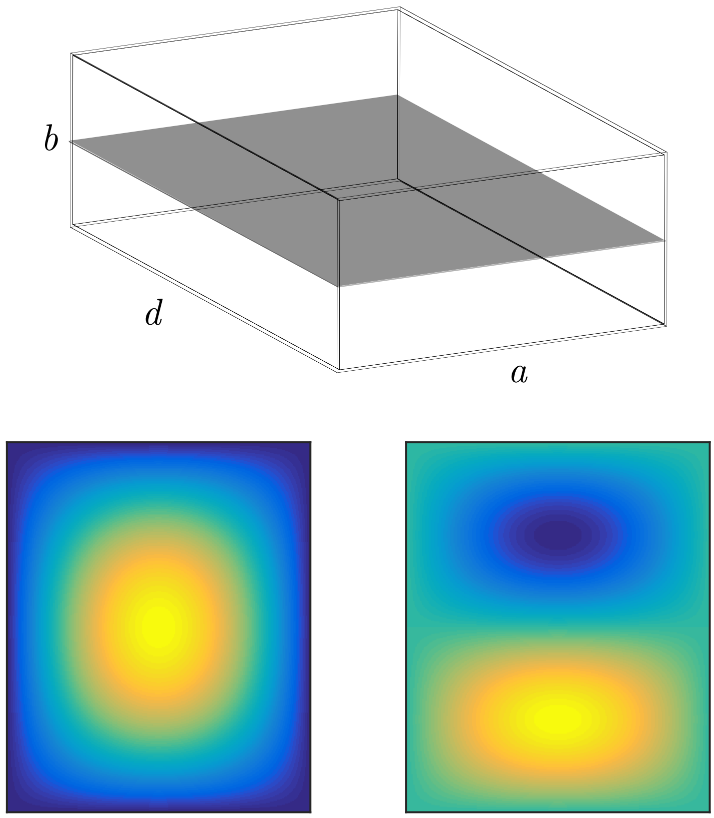

Figure 2.9: Schematic of a rectangular cavity resonator (top). Electric field distribution of the TE_{101} (bottom left) and TE_{102} (bottom right) modes on the schematic cutplane. The field is polarized perpendicular to the figure plane.

We may express this as

$$S_{ij} = \left.\frac{V_i^-}{V_j^+}\right|_{V_k^+=0,\ k\neq j}. \tag{2.19}$$

A network without active components, such as circulators or amplifiers, has a symmetric scattering matrix. Furthermore, if the S-matrix is non-unitary, this indicates internal losses are present in the network.

Cavities with one input and one output port may be regarded as a two-port network in scattering matrix analysis. From the S-parameters we can determine the quality factor and its internal and external components. The ratio of incident to transmitted power is given by $|S_{21}|^2$. Therefore $|S_{21}(\omega)|^2$ will describe a Lorentzian lineshape as plotted in Fig. 2.8, providing the resonator quality. The external and internal loss components may be determined by accounting for the amplitude reflected back at the input. For a two-port network they are related by [17]

$$Q_{\text{int}} = (1 + k_1 + k_2)Q. \tag{2.20}$$

The coupling coefficients k_i quantify the how strongly port i is coupled to the system environment. They are given by the scattering parameters at the resonance frequency f_r:

$$k_i = \frac{|S_{21}(f_r)|^2}{1 - |S_{ii}(f_r)|^2 - |S_{21}(f_r)|^2}. \tag{2.21}$$

Measuring the magnitudes of the reflected and transmitted signals of a two-port cavity will thus enable characterization in terms of internal and external quality, as well as the coupling coefficients. Assuming the cavity is connected to the environment in a symmetric fashion ($k_1 = k_2$), it is sufficient to record the scattering amplitudes $|S_{21}|$ and $|S_{11}|$.

2.4 Cavity QED and 3D circuit QED

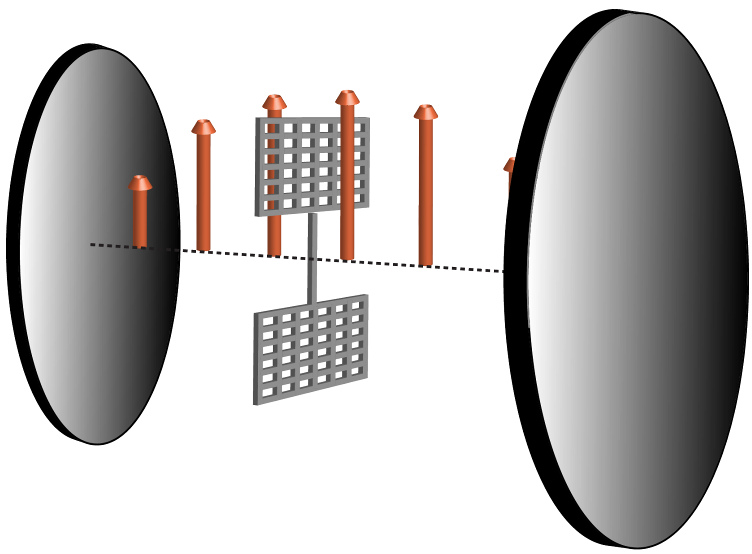

Figure 2.10: 3D cQED schematic

We are now ready to examine the combined system of qubit and resonator. The theory describing the interaction between a two-level system and a quantized electromagnetic field was first developed in the context of cavity quantum electrodynamics (cavity QED) [18]. Rather than artificial qubits, cavity QED involves atoms coupled to light fields in optical cavities, a research field that notably lead to the 2012 Noble Prize in physics being awarded to Serge Haroche and David Wineland [19]. Starting out with a discussion of the fundamental model of this interaction, the Jaynes-Cummings model, we then apply this formalism to the transmon. Finally, we describe in greater detail the physics behind the coupling of the transmon to the microwave field. Figure 2.10 shows a schematic drawing of the interaction involved in this 3D circuit QED picture, with a transmon qubit polarized by an electric field confined between two mirrors.

2.4.1 Jaynes-Cummings model

The quantum mechanical interaction between a two-level atom and a single resonant cavity mode gives rise to the well known Jaynes-Cummings Hamiltonian. As two-level systems are generally described using Pauli matrices, the atomic state enters the Hamiltonian as $\hat{H}_a = (\hbar\omega_a/2)\,\hat{\sigma}_z$. The resonator mode is described by a quantum harmonic oscillator and appears as $\hat{H}_r = \hbar\left(\hat{a}^\dagger\hat{a} + 1/2\right)$. The non-trivial dynamics of the system arise due to a third term in the Hamiltonian, accounting for the coupling of the atomic dipole moment of the atom and the cavity electric field. The electric field operator corresponds to the position operator of the harmonic oscillator. Ignoring quickly oscillating terms, this gives $\hat{H}_{\text{int}} = \hbar g\left(\hat{a}\hat{\sigma}^+ + \hat{a}^\dagger\hat{\sigma}^-\right)$, where $\hat{\sigma}^+$ ($\hat{\sigma}^-$) is the raising (lowering) operator for the atomic state. The strength of the interaction is given by the parameter g, the coupling strength, which provides a characteristic angular frequency for the exchange of energy between atom and cavity. We will find reason to return to this important quantity below. For $g \ll \omega_q,\, \omega_r$ and ignoring any losses or decoherence, we obtain

$$\hat{H} = \frac{\hbar\omega_a}{2}\hat{\sigma}_z + \hbar\omega_r\left(\hat{a}^\dagger\hat{a} + \frac{1}{2}\right) + \hbar g\left(\hat{a}\hat{\sigma}^+ + \hat{a}^\dagger\hat{\sigma}^-\right). \tag{2.22}$$

In 3D circuit QED, a qubit placed inside a cavity resonator is substituted for the atom, but the dynamics of the system still obey Eq. (2.22). For the transmon qubit however, the low anharmonicity may require taking higher qubit levels into account in certain parameter ranges.

For the Jaynes-Cummings Hamiltonian to describe well the time evolution of a 3D circuit QED system, it is necessary to reach the strong coupling limit, where the coupling strength is larger than the qubit decay and cavity loss rates ($g > \kappa,\ \Gamma_1,\ \Gamma_2$). Otherwise, the non-Hermitian interaction with the environment will dominate the system dynamics.

2.4.2 Dispersively coupled transmon

The time evolution generated by Eq. (2.22) differs considerably depending on whether the qubit frequency is near the cavity resonance. If the magnitude of the detuning $\Delta \equiv \omega_q - \omega_r$ is smaller than the coupling strength, the first excited state of the system will see energy being coherently transferred back and forth between qubit and resonator. Thus, neither a ground state qubit with a single cavity photon, nor an excited state qubit in an empty cavity are eigenstates of the system. The system investigated below (cf. Sec. 4.2) couples the cavity to a qubit whose first transition frequency is far detuned from the fundamental mode. This parameter range, where $\Delta \gg g$, is known as the dispersive regime. The large detuning inhibits the exchange of energy between qubit and resonator, resulting in eigenstates close to their bare parameters. Figure 2.11 shows how the state of an initially excited qubit evolves depending on the detuning in an ideal picture without decay or resonator losses. For an open system, with losses and decoherence induced by the environment, the time evolution of mixed states is described using density matrix formalism [20], incorporating Lindblad operators for the decay [21]. For a review of the dynamics of such systems, see Ref [22].

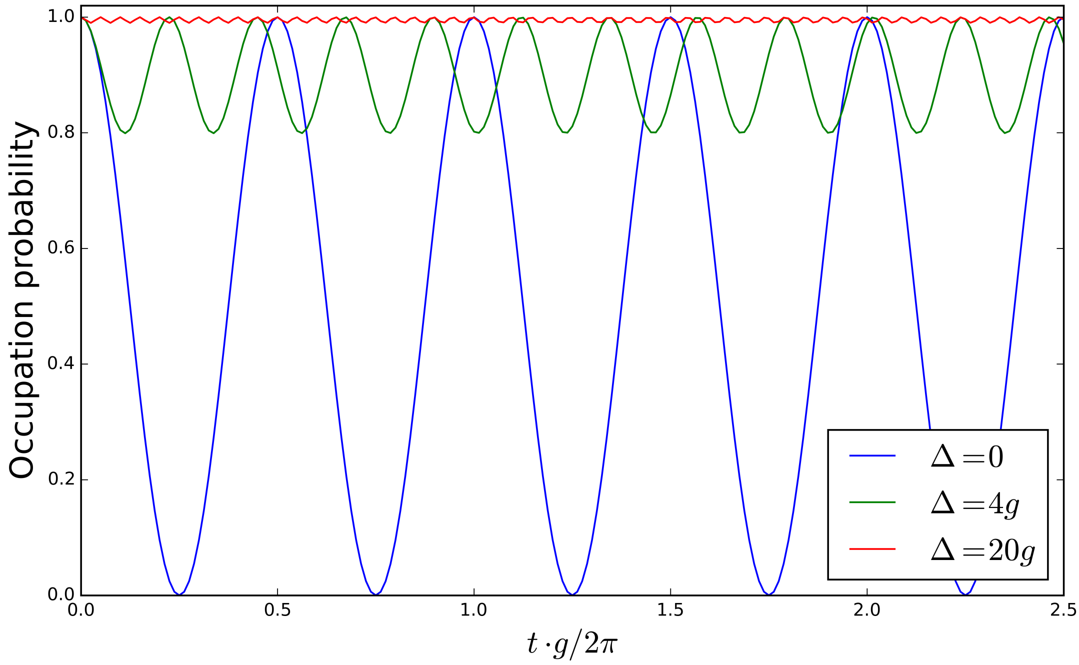

Figure 2.11: Time evolution of the qubit excited state occupation in the Jaynes-Cummings model for different values of the detuning simulated using QuTiP. The resonant case leads to the entire excitation energy oscillating between qubit and cavity. In the detuned limit, the exchange of energy is blocked almost completely.

In the dispersive limit, a unitary transformation may be applied to eliminate the coupling. The deviations from the bare, uncoupled qubit and resonator parameters can then be obtained from perturbation theory. In the two-level approximation this yields an effective Hamiltonian [23]

$$\hat{H}_{\text{eff}} = \hbar \left(\omega_r + \frac{g^2}{\Delta} \hat{\sigma}_z \right) \hat{a}^\dagger \hat{a} + \frac{\hbar}{2} \left(\omega_q + \frac{g^2}{\Delta} \right) \hat{\sigma}_z. \tag{2.23}$$

We note how the cavity field deviates from the bare resonator by the qubit state dependent shift of $\pm g^2/\Delta$. Known as the dispersive shift, this allows readout of the qubit state via the cavity. Grouping together terms in Eq. (2.23) acting on the qubit state, we obtain the qubit frequency in the composite system as

$$\omega_{01} = \omega_q + 2\frac{g^2}{\Delta} \left(\hat{a}^\dagger \hat{a} + \frac{1}{2} \right). \tag{2.24}$$

Qubit and resonator states and frequencies in the combined system are often referred to as the *dressed* state frequencies. This is a way to distinguish the composite eigenstates from the parameters of the isolated qubit and cavity.

For the transmon in the dispersive regime, the moderate anharmonicity may lead to higher qubit transitions affecting the dispersive shift of the cavity. In second order perturbation theory, the second transmon level also appears in the Hamiltonian. The result is a reduced dispersive shift and the effective Hamiltonian

$$\hat{H}_{\text{eff}} = \hbar\left(\omega_r - \frac{\chi_{12}}{2} + \chi\hat{\sigma}_z\right)\hat{a}^\dagger\hat{a} + \frac{\hbar}{2}\left(\omega_q + \chi_{01}\right)\hat{\sigma}_z. \tag{2.25}$$

We introduced here the interaction parameters

$$\chi = \chi_{01} - \chi_{12}/2 \tag{2.26}$$

$$\chi_{ij} = \frac{g^2}{\Delta_i} \tag{2.27}$$

where $\Delta_i \equiv \omega_{i-1,1} - \omega_r$ is the detuning between the ith transition and the resonator. Combining these expressions, the coupling strength can be determined from a recorded dispersive shift as

$$g = \left(\frac{\chi}{\frac{1}{\Delta_1} - \frac{1}{2\Delta_2}}\right)^{1/2}. \tag{2.28}$$

This relation allows for measurement of g via the cavity in a photon number independent way. It is therefore highly useful for determining the coupling strength and calibrating the photon number population of the cavity.

Since, as illustrated in Fig. 2.11, the qubit-resonator detuning prevents the qubit from decay by emitting a photon into the cavity mode, it is reasonable to expect an effect on the characteristic decay time T_1. By Fermi's golden rule, the rate of spontaneous emission of an excited state, the vacuum rate of photon emission decay, is given by [24]

$$\Gamma = 2\pi g\left(\omega\right)^2 D\left(\omega\right). \tag{2.29}$$

This rate depends on the final photon density of states D. Whereas in free space, the volume normalized density of states writes

$$D\left(\omega\right) = \frac{\omega^2}{\pi^2 c^3}, \tag{2.30}$$

the cavity Lorentzian filtering leads to an approximate expression for high Q resonators

$$D\left(\omega\right) = \frac{1}{\pi}\frac{\kappa/2}{\left(\omega - \omega_r\right)^2 + \left(\kappa/2\right)^2}. \tag{2.31}$$

This leads to a strong modulation of the decay rate due to the cavity impact on the photon density of states. For a qubit resonant with the cavity, the decay rate equals g in the strong coupling limit, much larger than the free space decay rate Γ_{free}. For qubits or atoms resonantly coupled to a cavity, the parameter g determines the rate of exchange of energy between them. This is one of the reasons why resonators are important to the study of light-matter interaction.

In the far detuned limit the decay rate is instead suppressed by the Lorentzian filtering of the cavity. Compared to the free space value, it is reduced by a factor depending on Q as well as a geometry factor.

$$\Gamma = \Gamma_{\text{free}} \frac{3}{16\pi^2 Q} \frac{\lambda^3}{V} \tag{2.32}$$

This coefficient is known as the Purcell factor and the associated effect is called the Purcell effect, after their discoverer E.M. Purcell [25]. A consequence of the Purcell effect is that high quality resonators can be used to increase coherence times. This entails a compromise with respect to measurement, as a high total Q requires the coupling of the cavity to the measurement setup to be weak. High internal quality is however always preferable. Since reaching high Q_{int} is typically easier with 3D cavities than planar structures, the longest qubit coherence times have been recorded in such configurations.

It is clear that the system dynamics differ substantially depending on the cavity-qubit detuning. With a split junction transmon as outlined in Fig. 2.7 and a some means of applying external magnetic flux through the loop, it is possible to tune the experiment continuously and in situ between the dispersive and resonant limits.

2.4.3 The coupling strength

In the Jaynes-Cummings model, the electric field couples to the dipole moment of the atom. The characteristic coupling strength per photon g is given by

$$g = \frac{\mu E_{\text{rms}}}{\hbar} \tag{2.33}$$

where μ is the expectation value of the dipole moment operator $-e\mathbf{r}$ applied to the atomic state and E_{rms} the root mean square of the vacuum electric field.

For the 3D transmon, μ is given by the dipole moment of the qubit structure where the Cooper pair charge $2e$ has been displaced from one pad to the other [26]. This dipole moment couples to the y-component of the vacuum RMS electric field of the first cavity mode at the qubit position. With electromagnetic FEM computations, we are able to compute these quantities and provide an a priori estimate for the coupling strength.

The vacuum electric field fluctuations for a single mode is given by [27]

$$E_{\text{rms}} = \sqrt{\frac{\hbar\omega}{2\epsilon_0 V}}. \tag{2.34}$$

Taking V to be the cavity volume would imply the assumption that the field is evenly distributed inside the cavity. A more rigorous consideration takes into account the field distribution of the fundamental cavity mode and relates it to the field at the qubit position. Instead of the cavity volume, we calculate the *mode volume* of the first resonant cavity mode, which we define as

$$V_{\text{mode}} = \frac{\int_V \epsilon\left(\mathbf{r}\right) \mathbf{E}^2\left(\mathbf{r}\right) \mathrm{d}^3 r}{\epsilon\left(\mathbf{r}_q\right) \mathbf{E}^2\left(\mathbf{r}_q\right)}. \tag{2.35}$$

Here, $\mathbf{r}_q$ refers to the qubit position inside the cavity. As the transmon is small compared to the fundamental mode wavelength, its dimensions may be disregarded for this analysis. For a rectangular cavity with homogeneous dielectric constant and side lengths a,b and d, integrating the analytical expression for the TE_{101} mode gives $V_{\text{mode}}/(abd) = 1/4$. An approach to refine this figure would be to use a numerical simulation more accurately representing the experimental design. Obtaining the electrodynamic parameters μ and V_{mode} in this manner, we may obtain an estimate of the coupling strength from

$$g = \mu \sqrt{\frac{\omega}{2\hbar\epsilon_0 V_{\text{mode}}}}. \tag{2.36}$$

In cavity QED with atoms, coupling strengths rarely exceed $g/2\pi = 20\,\mathrm{MHz}$. As it has a much larger dipole moment, the transmon couples much more strongly to the electric field. For transmons coupled to 3D cavities, couplings $g/2\pi > 100\,\mathrm{MHz}$ have been observed. With typical decay rates $\Gamma_1/2\pi$ on the order of 1MHz, 3D transmon configurations are usually not difficult to operate in the strong coupling regime.